Journal of Energy Chemistry 42 (2020) 56–61

Contents lists available at ScienceDirect

Journal of Energy Chemistry

journal homepage: www.elsevier.com/locate/jechem

http://www.journals.elsevier.com/journal-of-energy-chemistry/

Synthesis of mechanically robust porous carbon monoliths for CO_2 adsorption and separation

Jie Du, Wen-Cui Li, Zhan-Xin Ren, Li-Ping Guo, An-Hui Lu*

State Key Laboratory of Fine Chemicals, School of Chemical Engineering, Dalian University of Technology, Dalian 116024, Liaoning, China

ARTICLE INFO

Article history:
Received 9 May 2019
Revised 13 June 2019
Accepted 13 June 2019
Available online 22 June 2019

Keywords:
Carbon monoliths
High mechanical strength
Adsorption
Gas separation

ABSTRACT

Porous carbon materials with developed porosity, high surface area and good thermal- and chemical-resistance are advantageous for gas adsorption and separation. However, most carbon adsorbents are in powder form which exhibit high pressure drop when deployed in practical separation bed. While monolithic carbons have largely addressed the pulverization problem and preserved kinetics and usually suffer from abrasion during multiple adsorption-desorption cycles. Herein, we proposed the designed synthesis of mechanically robust carbon monoliths with hierarchical pores, solid nitrogen-containing framework. The synthesis started with the polymerization of resorcinol and formaldehyde under weakly acidic conditions generated from cyanuric acid, and then an appropriate amount of hexamethylenetetramine (HMTA) was added as a crosslinker to prompt the formation of three dimensional frameworks. After carbonization process, the as-obtained porous carbon monoliths have a high radial compressive strength of 886 N/cm as well as a BET specific surface area of up to 683 m^2/g. At approximately 1 bar, the CO_2 equilibrium capacities of the monoliths are in the range of 3.1–4.0 mmol/g at 273 K and of 2.3–3.0 mmol/g at 298 K, exhibiting high selectivity for the capture of CO_2 over N_2 from a stream which consists of 16.7% (v%) CO_2 in N_2. Meanwhile, they undergo a facile CO_2 release in an argon stream at 298 K, indicating a good regeneration capacity. After cycle testing, sieving and regeneration, the adsorbent has no mass loss, compared to that of its fresh counterpart.

1. Introduction

The selective capture and separation of carbon dioxide (CO_2) in an economical and energy-efficient method has attracted tremendous attention, due to the dual roles of CO_2 as a greenhouse gas and a renewable carbon source. It is considered advantageous to capture carbon dioxide by adsorption technology because of its simple equipment and process, low energy consumption, and no corrosion to equipment. The key to the adsorption process is the design of the efficient adsorbent material. In recent years, a number of CO_2 capture porous solids have been developed, including porous carbons, zeolites (e.g., 13X, 5A, natrolite), amine-modified silicas, and new classes of hybrid crystalline solids (e.g., MOFs, ZIFs, COFs, MCPs, PCPs). Among them, porous carbons are most suitable for CO_2 capture used in a wide range of operating conditions because of high surface area, chemical stability, thermal stability and wide availability [1].

Carbon monoliths are the most promising carbon forms with 3-D framework structures consisting of interconnected carbon particles [2]. They not only have many properties common to activated carbon mentioned above, but also exhibit several favorable properties, such as low pressure drop, short diffusion lengths and no thermal shock resistance, which benefit from monolithic structures they have [3]. These advantages made carbon monoliths attract many interests in various applications, ranging from catalysis, adsorption, sensing, and separation to biotechnology and more desirable than carbon powders [4].

Generally, monolithic carbon materials are prepared via structuring process of activated carbon powders or carbon precursors with binders before high-temperature pyrolysis [5]. For example, Gao et al. [6] selected mesophase pitch as carbon precursor and binder admix with coal particles and KOH to make a paste. After pressing and pyrolysis, activated carbon discs were obtained. Thiruvenkatachari et al. [7] used a vacuum molding unit to obtain

* Corresponding author.
E-mail address: anhuilu@dlut.edu.cn (A.-H. Lu).

https://doi.org/10.1016/j.jechem.2019.06.006

a honeycomb monolith made of carbon fiber and powdered phenolic resin as a binder. A honeycomb monolithic carbon was finally fabricated. Preparation process of carbon monoliths via structuring process has been intensively investigated. However this method has a general disadvantage that the addition of binders usually leads to partial loss of the porosity of the monolith [8].

Another route to synthesize monolithic carbon materials via carbonization of monolithic polymers which are synthesized through the polymerization like phenolic resin has attracted more attention. Gomis-Berenguer et al. [9] synthesized carbon xerogels with ultrahigh micro- and mesopores from the activation of polymeric resins prepared by polycondensation of resorcinol/formaldehyde mixtures in basic medium and subcritical drying. Macías et al. [10] prepared flexible monolithic carbon aerogels by incorporating diatomite as anti-shrinkage agent during the sol-gel polycondensation of resorcinol and formaldehyde. However, the mechanical strength of the carbon aerogel is far from being able to meet the practical application requirements.

As well known, thermosetting resins or thermoplastic phenolic resins can be obtained by polymerization of phenols and aldehydes on either alkaline or acidic conditions [11]. The usage of a base catalyst results in the formation of a thermosetting resin, which has a rigid, three-dimensional structure owing to crosslinked linear molecules. When an acid catalyst is used, a thermoplastic resin will be obtained. The thermoplastic resin consists of linear molecules and is a state of a polymer in which the molecules have not been crosslinked to form a three-dimensional structure. Those carbon monoliths obtained from thermoplastic resins often exhibit cracking, high shrinkage and almost no specific surface area, but have an extremely high hardness. Empirically, monolithic carbons pyrolyzed from thermosetting resins are more likely to yield monoliths with no crack, low shrinkage, and high porosity. In our previous work, we reported that resorcinol, formaldehyde and amine were copolymerized in an alkaline condition to get a thermosetting resin. After carbonization at a high temperature, the monolithic carbon with a 3D network structures, high specific surface and interpenetrating porosity was obtained [12,13]. However, the remained problem is that the carbon monolith prepared is unsatisfactory in mechanical strength.

By considering the respective characteristics of thermoplastic and thermosetting resins and keeping in mind that thermoplastic resins can be transformed to thermosetting resins using a crosslinker such as hexamethylenetetramine [14], herein we reported a novel route to prepare a carbon monolith with both high compressive strength and desirable porosity. Differing from the previous often reported the phenol-aldehyde polymerization system under alkaline conditions, resorcinol was firstly polymerized with formaldehyde under a weakly acidic condition and then an appropriate amount of hexamethylenetetramine (HMTA) was added as a crosslinker to prompt a transformation of thermoplastic resin to thermosetting resin partially. After carbonization, the carbon monoliths have a radial compressive strength of 886 N/cm and a BET specific surface area of up to 683 m^2/g. A column breakthrough experiment of mixture streams CO_2/N_2 (16.7/83.3 v/v) was carried out at 298 K and 1.1 bar, in order to test the separation performance of this carbon monolith as an adsorbent for CO_2.

2. Experimental

2.1. Chemicals

The following materials were used as received without further purification. Resorcinol, formaldehyde and potassium carbonate (K_2CO_3) were supplied by Sinopharm Chemical Reagent Co., Ltd. Cyanuric acid (CA) and hexamethylenetetramine (HMTA) were purchased from Aladdin Industrial Corporation.

2.2. Synthesis of porous carbon monoliths

Monolithic porous carbon was synthesized by polymerization of resorcinol and formaldehyde in the presence of cyanuric acid and hexamethylenetetramine as the catalyst and crosslinker respectively. A small amount of potassium carbonate was used to induce the dissolution of the cyanuric acid in formaldehyde. Firstly, CA was added in formaldehyde solution followed by 40 μL K_2CO_3 solution (5 mol/L) was added in during stirring, resulting in a clear solution A. Solution B contains resorcinol dissolved in water. Solution B was decanted into solution A with vigorous stirring to obtain a homogeneous solution. The pH of the solution was close to 6.5. After HMTA was added and dissolved, the clear homogeneous system was sealed and transferred into oven at 363 K to cure for 4 h. The as-made polymer was dried at room temperature for 48 h followed by further drying which operated at 323 K for 72 h before obtaining an orange polymer monolith. Finally, porous carbon was obtained by pyrolysis of the polymer at 1073 K for 2 h, with a heating rate of 2 °C/min. By changing the amount of CA and HMTA, a series of polymer monoliths were prepared. In all cases, the molar ratio of R/F was fixed as 1:2 and the amount of K_2CO_3 was fixed.

2.3. Characterization

Scanning electron microscope (SEM) images were obtained with a Hitachi UHR FE-SEM SU8200 instrument. Transmission electron microscopy (TEM) images were obtained with a 200 kV Tecnai G220S-Twin electron microscope equipped with a cold field emission gun. Roughness measurements were carried out by a Taylor Hobson 120 mm PGI-840 phase grating interferometer. Compressive strength tests were carried out by a DL-4 intelligent particle strength tester with a maximum range of 2000 N. Nitrogen sorption isotherms were measured with an Autosorb-iQMP automated gas sorption analyzer (Quantachrome). The Brunauer– Emmett–Teller (BET) method was used to calculate the specific surface areas (S_{BET}). Pore size distributions (PSDs) were determined from the adsorption branches of the isotherms using QSDFT method for micropores. Total pore volumes (V_{total}) were calculated from the amount adsorbed at a relative pressure P/P_0 of 0.95. Micropore volumes (V_{micro}) were calculated using the t-plot method. Carbon dioxide adsorption isotherms at 273 K were measured with an ASAP 2020 sorption analyzer (Micromeritics) and pore size distributions for micropores (smaller than 0.5 nm) were determined from the adsorption branches of the isotherms using NLDFT method. Before measurements, carbon samples were degassed under vacuum at 473 K for 4 h. Elemental analysis was performed on a CHN elemental analyzer (Vario EL III, Elementar).

2.4. Equilibrium adsorption measurements

The gases equilibrium adsorption measurements were performed by using a Micromeritics ASAP 2020 static volumetric analyzer at the required temperature. Prior to each adsorption experiment, samples were degassed for 4 h at 473 K and then cooled down to the required temperature, followed by the introduction of pure gas (N_2 at 99.99% and CO_2 at 99.995% purity) into the system. The gas adsorption capacity in terms of adsorbed volume under standard temperature and pressure (STP) was then recorded. The isosteric heat of adsorption Q_{st} was calculated by using the Clausius–Clapeyron equation: $Q_{st} = RT^2 (\partial \ln P/\partial T)_q$, in which R is the universal gas constant, T is the absolute temperature, P is the equilibrium pressure, and q is the amount adsorbed.

2.5. Dynamic gas separation measurements

The column breakthrough experiments of mixture streams CO_2/N_2 (16.7/83.3 v/v) were carried out at 298 K and 1.1 bar in a fixed-bed flow sorber (a stainless-steel tube with an inner diameter of 8.0 mm and the packed length was 120 mm). Thermal pretreatment of sample was conducted at 393 K for 12 h before dynamic adsorption experiments. The particle size is about 40–60 mesh. The adsorbent bed was first heated at 358 K in Ar at a flow rate of 100 mL/min for 2 h. Then, breakthrough experiments were performed by switching abruptly from Ar to a gas mixture of CO_2/N_2 at a flow rate of 12 mL/min. A sample saturated with gas molecules was subjected to an Ar flow of 30 mL/min at 298 K. After 20 min, no gas molecule was detected in the effluent. The effluent gas was monitored online by using an Agilent 7890A gas chromatograph with a thermal conductivity detector (TCD). Gas cycling experiments were carried out under the same conditions for ten times. After gas cycling experiments, the adsorbents were collected and sieved with a 60 mesh sieve, then recovered at 393 K for 12 h and recorded the quality.

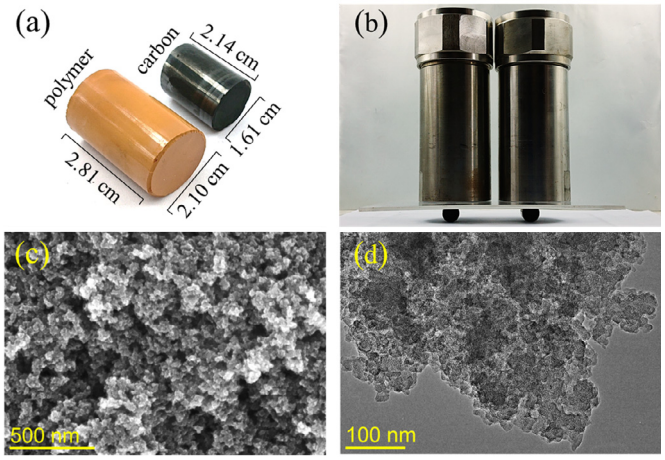

Fig. 1. (a) Photograph of as-made polymer monolith and its carbonized product, (b) photograph of CRF-3 being pressed by autoclaves, (c) SEM and (d) TEM images of CRF-3.

3. Results and discussion

3.1. Structural properties of the synthesized carbon monoliths

Fig. 1(a) is an optical photograph of the polymer and carbon monolith prepared in the typical case, as can be seen from the photograph, an essentially crack-free carbon monolith was prepared and the shape is consistent with the polymer. However, the volume shrinkage is 55.4 vol% while linear shrinkage along the longitudinal and the radial are 23.8% and 23.2%, respectively, indicating that the structure of the polymer converted to carbon uniformly [13]. The roughness (*Ra*) of the side and bottom surfaces of carbon monolith is 0.04 μm and 0.84 μm, respectively, which is determined by the wall of the glass tube reactor and the silicone plugs. And the *Ra* of the cross-section is 0.66 μm, which is most representative, meaning a smooth surface. Smaller surface roughness can reduce wear by reducing the friction of the interfaces [15]. The as-prepared carbon monolith can well retain the surface roughness of the mould, making the roughness of the monolith adjustable according to requirements, which is favorable in further application. Fig. 1(b) is a photograph of CRF-3 being pressed by outer linings of autoclave which is made of stainless steel and each weighing approximately 3 kg, showing the compressive strength of the sample. It can be seen from the scanning electron microscopy (SEM) image (Fig. 1c) that the skeleton of sample CRF-3 is composed of homogeneously interconnected spherical units. This makes the carbon framework of the carbon monolith full of macropores, which is beneficial to the diffusion of guest molecules. Transmission electron microscopy (TEM) image of CRF-3 (Fig. 1d) reveals that the carbon framework is composed of nano-scale particles, which is consistent with SEM characterization.

Table 1 lists the macroscopic structure parameters of a series of prepared carbon monoliths. As the amount of CA increases, the volume shrinkage of carbon monoliths decreases. CRF-1 with the lowest CA content had only one small block left after carbonization. The volume shrinkage gradually approaches 50% as the amount of CA increases. The increased amount of CA results in more reaction sites, allowing the formation of 3D interconnected skeleton and thus reduces the shrinkage of the material. Although the carbon yield is gradually reducing, it maintains at about 50%, an acceptable level [16]. The bulk density and the radial compressive strength also show same trend. The compressive strength of CRF-1 and CRF-2 exceeds the testing range of the instrument, while CRF-1 has the highest bulk density and compressive strength, which is related to its high shrinkage. The compressive strength of samples CRF-4 and CRF-5 shows a cliff-like decline. CRF-3 as the typical sample has the advantages of appropriate volume shrinkage of 55.4%, carbonization yield of 48.7 wt%, bulk density of 0.465 g cm^{-3}, and high compressive strength which is 886 N/cm.

The N_2 sorption isotherms of all samples are shown in Fig. 2(a). It can be seen that at very low P/P_0, there is a steep uptake, indicating their microporous characteristics. When the pressure goes higher, the isotherms of samples CFR-1, CFR-2 and CFR-3 exhibit a hysteresis at the relative pressure above 0.8, indicating the existence of mesopores and macropores [17]. As the used amount of CA increases, the specific surface area of the samples increases first and then decreases (Table 2), while CFR-3 has the largest surface area reaching 683 m^2/g. The total pore volume decreases as the CA content increases, while the micropore pore volume has an opposite tendency, meaning the increase of the proportion of micropores. The elemental analyses show that nitrogen content reaches a maximum 1.42 wt% of CRF-1, which ensures an improved adsorption performance for acidic gases, and further increase in CA content leads to a decrease in nitrogen content [18–20]. The PSDs (Fig. 2b and c) show that the majority of the micropores are concentrated around 0.5 nm and a broad range distribution of mesopores. In order to characterize the smaller micropores (smaller than 0.5 nm), a CO_2 adsorption isotherm was measured and shown in Fig. 2(d). Fig. 2(e) shows the PSD from the CO_2 (solid) and the N_2 (hollow) sorption isotherms. It can be seen that there are two distribution peaks at 0.36 nm and 0.52 nm.

Table 1. Macroscopic structure parameters of carbon monoliths.

Sample	Bulk shrinkage (vol%)	Carbon yield (wt%)	Bulk density (g/cm^3)	*P* (N/cm)
CRF-1	74.2	52.0	0.818	>1090
CRF-2	64.5	50.6	0.580	>978
CRF-3	55.4	48.7	0.465	886
CRF-4	51.9	47.8	0.423	146
CRF-5	50.4	46.3	0.417	153

Table 2. Physical and chemical characteristic of the synthesized carbon monoliths.

Sample	Physical properties				Chemical properties			
	S_{BET} (m^2/g)	S_{micro} (m^2/g)	V_{total}* (cm^3/g)	V_{micro} (cm^3/g)	N (wt%)	C (wt%)	H (wt%)	O (wt%)
CRF-1	595	211	0.80	0.094	1.42	83.94	1.81	12.83
CRF-2	670	173	0.94	0.079	1.36	83.76	1.87	13.01
CRF-3	683	241	0.76	0.108	1.27	83.60	1.93	13.20
CRF-4	626	274	0.53	0.119	1.10	83.69	1.98	13.23
CRF-5	621	266	0.48	0.116	1.11	81.79	2.07	15.03

* $P/P_0 = 0.95$.

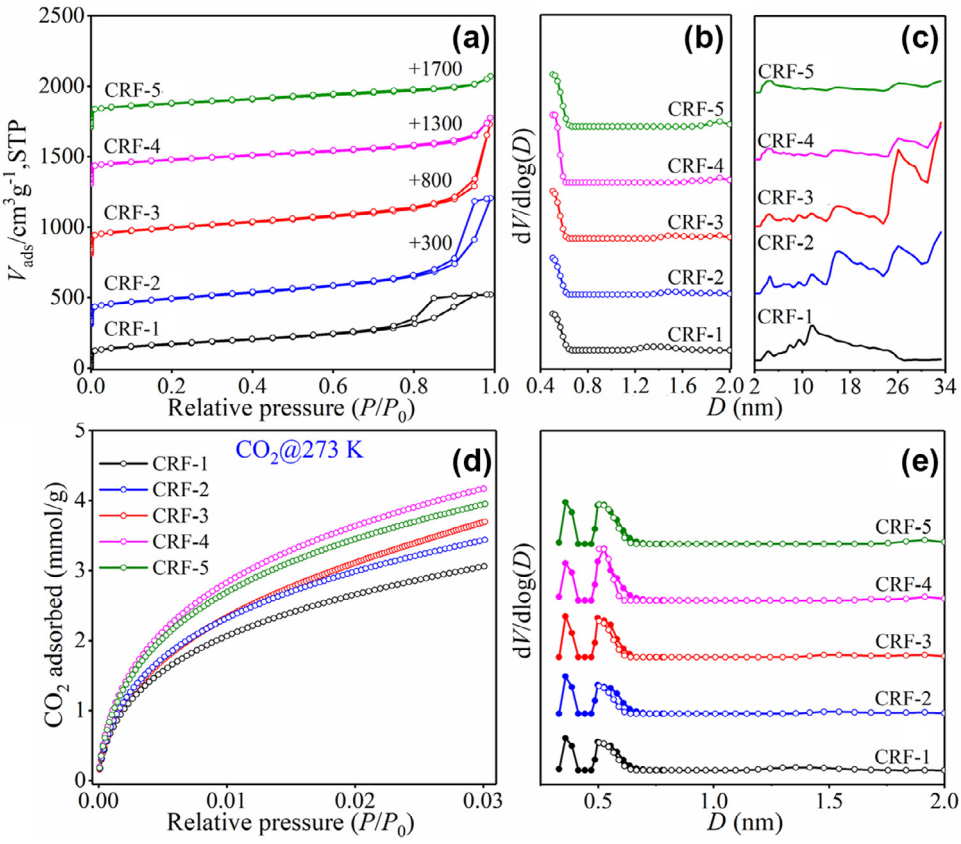

Fig. 2. (a) N_2 sorption isotherms of the carbon monoliths and (b,c) the corresponding PSDs calculated using the DFT method, (d) CO_2 sorption isotherms at 273 K of samples and (e) the corresponding PSDs calculated using the DFT method.

The distribution curves derived from CO_2 (solid) and N_2 (hollow) sorption isotherms are in good consistent when the pore sizes are greater than 0.5 nm. These micropores play an important function in adsorption and separation of CO_2 (0.33 nm in diameter) from a gas mixture because of the enhancement of the adsorption potential and molecular sieve effects.

3.2. CO_2 adsorption and separation by the carbon monoliths

The prepared carbon monoliths were evaluated in terms of equilibrium and dynamic CO_2 capacities, selectivity and other parameters such as adsorption thermodynamics, regenerability, and stability. The equilibrium CO_2 (at 273 and 298 K) isotherms of samples are accordingly shown in Fig. 3(a and b). The CO_2 adsorption capacity of samples shows an upward trend as the amount of CA increases, however, CRF-5 appears abnormal. In comparison, CRF-4 has the highest CO_2 adsorption capacity of 2.94 mmol/g at 1 bar, 298 K and 4.01 mmol/g at 1 bar, 273 K. The CO_2 adsorption capacity of CRF-3 at 1 bar is 2.65 mmol/g and 3.58 mmol/g at 298 K and 273 K respectively. The CO_2 adsorption capacity of the samples under different pressures is given in Table 3. By applying a variant of the Clausius–Clapeyron equation fitting the CO_2 adsorption isotherms measured at 273 K and 298 K, the isosteric heat of adsorption (Q_{st}) was calculated (Fig. 3c). For all samples, the isosteric heat of adsorption lies in the range of 20–30 kJ/mol and has a gentle trend, meaning a physical adsorption and uniform adsorption sites on the surface. Although CRF-3 is not the best sample from the static adsorption results, CRF-3 is more advantageous in view of the compressive strength discussed above. The obtained

Table 3. CO_2 adsorption capacity of carbon monoliths.

Sample	q_{ads} (mmol/g) at 298 K		q_{ads} (mmol/g) at 273 K	
	$P = 0.1$ bar	$P = 1.0$ bar	$P = 0.1$ bar	$P = 1.0$ bar
CRF-1	0.7	2.29	1.2	3.12
CRF-2	0.8	2.50	1.3	3.37
CRF-3	0.8	2.65	1.4	3.58
CRF-4	0.9	2.94	1.5	4.01
CRF-5	0.9	2.76	1.5	3.71

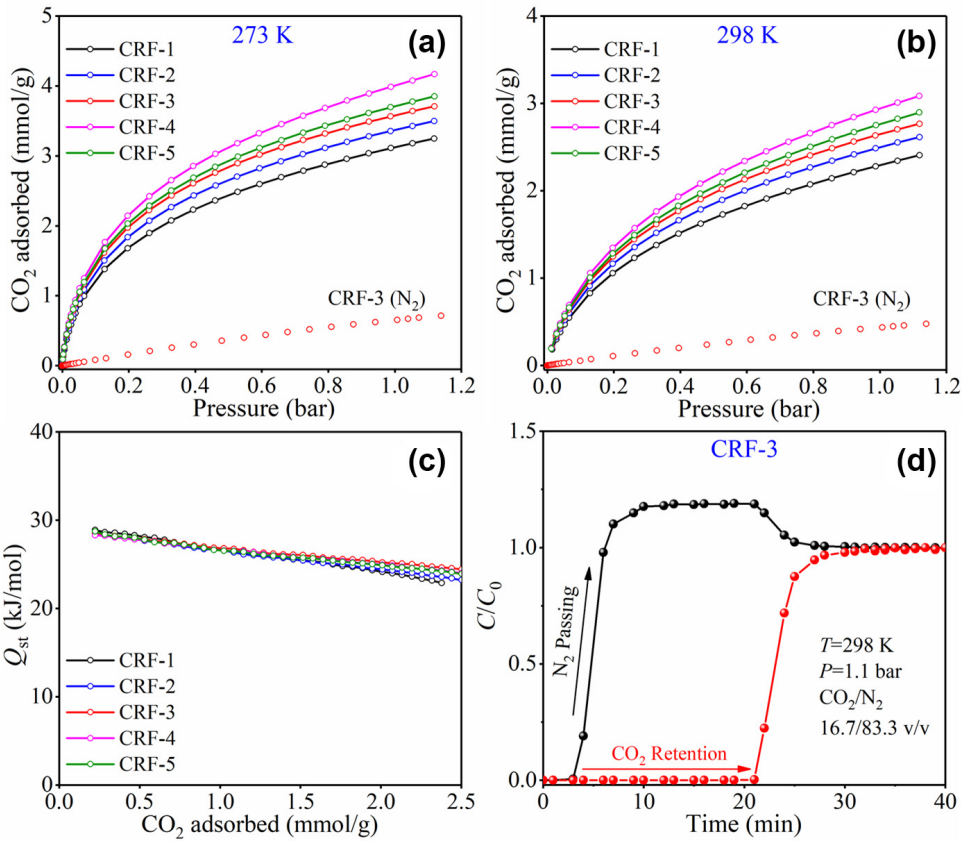

Fig. 3. (a) CO_2 adsorption isotherms of monoliths and N_2 adsorption isotherm of CRF-3 at 273 K, (b) CO_2 adsorption isotherms of monoliths and N_2 adsorption isotherm of CRF-3 at 298 K, (c) isosteric heat of adsorption for CO_2 at different CO_2 loadings, (d) breakthrough curves (a 16.7 vol% mixture of CO_2 in N_2 is fed into a bed of CRF-3).

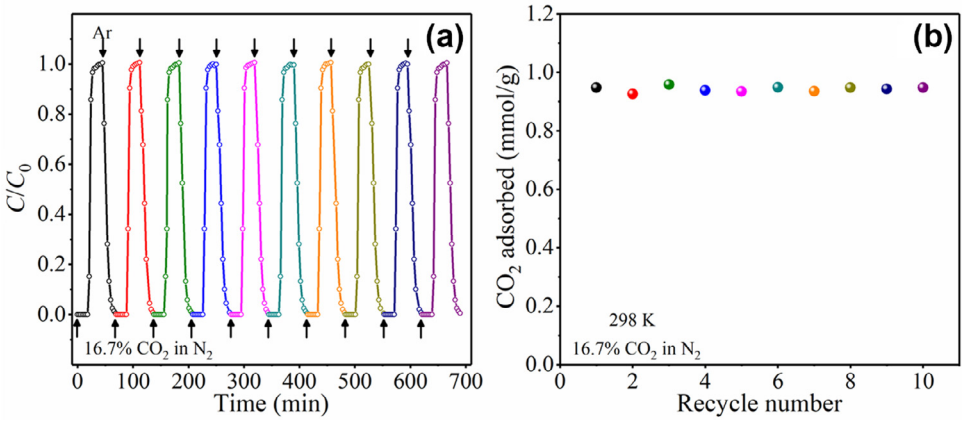

Fig. 4. (a) Recycle runs of CO_2 adsorption-desorption on CRF-3 at 298 K, using a stream of 16.7 vol% CO_2 in N_2, followed regeneration by Ar flow and (b) the adsorbed amount of CO_2 corresponding to each cycle.

"breakthrough curve" (Fig. 3d) demonstrates that the CRF-3 can completely separate CO_2 from the N_2 stream, and the estimated selectivity was close to infinite.

Gas cycling experiments verified the reversible CO_2 capture capacity of CRF-3. The sample saturated with CO_2 was purged with argon at 30 mL/min at 298 K. After ~15 min, no CO_2 was detected in the effluent (Fig. 4). Continuous regeneration experiments showed that under such mild regeneration conditions, CRF-3 retained 95%–99% of the intrinsic capacity. Further cycling did not cause a significant reduction in capacity, indicating that CRF-3 provided high-capacity separation with very mild regeneration conditions. This property makes it superior to many other porous solids such as zeolite [21], amine-modified silica [22,23], and MOFs [24] which would require thermal activation or vacuum regeneration. The distinctive regenerative properties of the material are more advantageous in practical applications. The recovered adsorbent after gas cycling experiment has almost no mass loss and indicates the high mechanical strength of the adsorbent.

4. Conclusions

In this study, we have synthesized mechanically robust carbon monoliths via a sol-gel method. The transformation of thermoplastic resin to thermosetting resin partially induced by CA and HMTA

ensures monolithic carbon a high radial compressive strength combining with desirable porosity. When used as an adsorbent, the carbon monolith shows good carbon dioxide adsorption and separation performance, outstanding regeneration property. We believe that this type of material may find more uses in the application areas of adsorption, catalysis and energy storage.

Acknowledgments

This project was financially supported by a Joint Sino-German Research Project (21761132011), the National Natural Science Foundation of China (No. 21776041) and the Cheung Kong Scholars Programme of China (T2015036).

References

[1] A.H. Lu, S. Dai, J. Mater. Chem. A 1 (2013) 9326.
[2] X. Jia, B. Dai, Z. Zhu, J. Wang, W. Qiao, D. Long, L. Ling, Carbon 108 (2016) 551–560.
[3] D. Guo, W. Li, W. Dong, G. Hao, Y. Xu, A.H. Lu, Carbon 62 (2013) 322–329.
[4] A.H. Lu, J.H. Smått, M. Lindén, Adv. Funct. Mater. 15 (2005) 865–871.
[5] F. Akhtar, L. Andersson, S. Ogunwumi, N. Hedin, L. Bergström, J. Eur. Ceram. Soc. 34 (2014) 1643–1666.
[6] S. Gao, B.S. Villacorta, L. Ge, K. Steel, T.E. Rufford, Z. Zhu, Fuel Process. Technol. 177 (2018) 219–227.
[7] R. Thiruvenkatachari, S. Su, H. An, X.X. Yu, Prog. Energ. Combust. 35 (2009) 438–455.
[8] W.C. Li, A.H. Lu, R. Palkovits, W. Schmidt, B. Spliethoff, F. Schüth, J. Am. Chem. Soc. 127 (2005) 12595–12600.
[9] A. Gomis-Berenguer, R. García-González, A.S. Mestre, C.O. Ania, Adsorption 23 (2017) 303–312.
[10] C. Macías, G. Rasines, T.E. García, C. Rodríguez, P. Lavela, J.L. Tirado, C.O. Ania, Carbon 98 (2016) 280–284.
[11] K. Nakagawa, S.R. Mukai, K. Tamura, H. Tamon, Chem. Eng. Res. Des. 85 (2007) 1331–1337.
[12] G. Hao, W. Li, D. Qian, A.H. Lu, Adv. Mater. 22 (2010) 853–857.
[13] G. Hao, W. Li, D. Qian, G. Wang, W. Zhang, T. Zhang, A. Wang, F. Schüth, H. Bongard, A.H. Lu, J. Am. Chem. Soc. 133 (2011) 11378–11388.
[14] J.P. Patel, S. Deshmukh, C. Zhao, O. Wamuo, S.L. Hsu, A.B. Schoch, S.A. Carleen, D. Matsumoto, J. Polym. Sci. Pol. Phys. 55 (2017) 206–213.
[15] L. Peña-Parás, H. Gao, D. Maldonado-Cortés, A. Vellore, P. García-Pineda, O.E. Montemayor, K.L. Nava, A. Martini, Tribol. Int. 119 (2018) 88–98.
[16] Z. Zou, C. Jiang, J. Porous Mat. 24 (2017) 1555–1564.
[17] M. Thommes, K. Kaneko, A.V. Neimark, J.P. Olivier, F. Rodriguez-Reinoso, J. Rouquerol, K.S. Sing, Pure Appl. Chem. 87 (2015) 1051–1069.
[18] A. Bagreev, J. Angel Menendez, I. Dukhno, Y. Tarasenko, T.J. Bandosz, Carbon 42 (2004) 469–476.
[19] F. Adib, A. Bagreev, T.J. Bandosz, Langmuir 16 (2000) 1980–1986.
[20] J.R. Pels, F. Kapteijn, J.A. Moulijn, Q. Zhu, K.M. Thomas, Carbon 33 (1995) 1641–1653.
[21] P.J.E. Harlick, F.H. Tezel, Micropor. Mesopor. Mat. 76 (2004) 71–79.
[22] X. Ma, X. Wang, C. Song, J. Am. Chem. Soc. 131 (2009) 5777–5783.
[23] C. Chen, S. Yang, W. Ahn, R. Ryoo, Chem. Commun. (2009) 3627–3629.
[24] G. Hao, W. Li, A.H. Lu, J. Mater. Chem. 21 (2011) 6447–6451.